

Short Communication

## Facile Synthesis of Hollow Co<sub>9</sub>S<sub>8</sub> Nanospheres for High Performance Pseudocapacitor

Liping Zhang, Yourong Wang, Wei Zhou, Guangsen Song and Siqing Cheng\*

Innovation Center for Nanomaterials in Energy and Medicine (ICNEM), School of Chemical and Environmental Engineering, Wuhan Polytechnic University, Hubei 430023, P. R. China

\*E-mail: [icnem@hotmail.com](mailto:icnem@hotmail.com)

Received: 3 November 2015 / Accepted: 26 November 2015 / Published: 1 January 2016

---

The hollow Co<sub>9</sub>S<sub>8</sub> nanospheres with ca. 50 nm were elaborately fabricated by a facile solvothermal method and characterized by powder X-ray diffraction (XRD), Scanning electron microscopy (SEM) and BET measurement to result in a specific surface area of 226 m<sup>2</sup> g<sup>-1</sup>. The prepared hollow Co<sub>9</sub>S<sub>8</sub> nanosphere electrode delivers a initial specific capacitance of 234.7 F g<sup>-1</sup> at a current density of 0.5 A g<sup>-1</sup>, which can be retained up to the 60<sup>th</sup> cycle, indicating the good cycleability and excellent rate capability. As a consequence, the energy density of the prepared Co<sub>9</sub>S<sub>8</sub> pseudocapacitor could reach up to 17.96 Wh kg<sup>-1</sup> at a power density of 32.82 W kg<sup>-1</sup>, which is much more than those of common electric double capacitors, exhibiting the pseudocapacitive characteristic. This might be due to the unique hollow Co<sub>9</sub>S<sub>8</sub> nanosphere structure to shorten the path of the electron transportation and the ionic diffusion.

---

**Keywords:** Co<sub>9</sub>S<sub>8</sub>; Hollow nanosphere; Electrochemical performance; Pseudocapacitor.

### 1. INTRODUCTION

Electrochemical capacitors (ECs), also known as supercapacitors, have received extensive attention for decades as a promising energy storage technology due to their high power density, long cycle life and rapid charging/discharging capability compared with conventional lithium-ion battery.[1-3] However, the limited energy density (~ 5 Wh kg<sup>-1</sup>) of ECs system restricts its applications to those demanded by ubiquitous electronic devices and electrical equipment.[4-5] As a consequence, many burgeoning efforts have been focused on fabricating new capacitor configuration and engineering new electrode materials for increasing both the specific capacitance C and the work voltage window V in terms of the energy density formula of  $E=(1/2)CV^2$ . [6-8] In this regard, the so-called pseudocapacitor is an efficient way because its energy storage relies on electric double layers

(non-Faradaic process) as well as via reversible oxidation – reduction (redox) reaction (Faradaic process) to achieve high specific capacitance.[9-13] Particularly, when combined with the electric double layer capacitor (EDLCs) to construct the hybrid pseudocapacitor[14-18], the pseudocapacitor would result in a wide work voltage window in aqueous electrolyte. Obviously, the active electrode materials for the pseudocapacitor with large specific surface area, high electrochemical active and negligible resistance are vital to improve the electrochemical properties of the pseudocapacitor. Therefore, many researchers are currently devoted to tactfully designing and fabricating the novel active electrode materials for the pseudocapacitive electrode.

Among the reported electrochemical electrode materials for the pseudocapacitor, the family of semiconductor cobalt sulfide such as  $\text{Co}_{1-x}\text{S}$ ,  $\text{CoS}$ ,  $\text{CoS}_2$  and  $\text{Co}_3\text{S}_4$  has been widely investigated [19-23] owing to their relatively high capacitance, high thermal and electric conductivity, low cost, fast redox kinetics and environment-friendly feature. As an important member, although  $\text{Co}_9\text{S}_8$  has been demonstrated potential in many other fields such as magnetic devices [24], optical sensors[25-27], catalysis[28-29] and lithium-ion battery[30], it is seldom reported as electrochemical active materials for the pseudocapacitor. Recently, Raghupathy et al. reported the applicability of the  $\text{Co}_9\text{S}_8$ /graphene nanocomposites for supercapacitor with a maximum specific capacitance of  $808 \text{ F g}^{-1}$ . [31] Wang et al. investigated the uniform  $\text{Co}_9\text{S}_8$  nanotube arrays on conductive nickel foam as the electrode for high performance supercapacitor, delivering a high rate capability of  $1483 \text{ F g}^{-1}$  at  $24 \text{ A g}^{-1}$ . [32] Fang et al. demonstrated three dimensional  $\text{Co}_9\text{S}_8$  nanorod@ $\text{Ni}(\text{OH})_2$  nanosheet core-shell structure on flexible carbon cloth as supercapacitor electrode material to achieve a high energy density of  $70.0 \text{ Wh kg}^{-1}$  at the power density of  $305.7 \text{ W kg}^{-1}$ . [33] All these manifest that  $\text{Co}_9\text{S}_8$  is a promising electrochemical active material for high performance supercapacitor only if its structure is rationally designed and elaborately fabricated.

Hereby, in this paper, we fabricated hollow  $\text{Co}_9\text{S}_8$  nanospheres using sublimed sulfur as sulfur source by a simple solvothermal method and investigated their electrochemical performance as supercapacitor electrode.

## 2. EXPERIMENTAL METHOD

### 2.1. Materials and Synthesis

All chemical reagents used here were of analytical grade, purchased from Sinopharm Chemical Reagent Co. Ltd. and used without further purification unless otherwise stated. In a typical experiment, 2 mmol of cobalt acetate was dissolved in 40 ml of absolute ethanol, followed by adding 2 mmol of sublimed sulfur. After vigorously being stirred for about 60 min, the resultant solution was transferred into 50 ml Teflon-lined stainless steel autoclave (with filling volume ratio of 80%), and then sealed and heated in a digital temperature –controlled oven at  $220 \text{ }^\circ\text{C}$  for 24 h. The obtained black  $\text{Co}_9\text{S}_8$  was collected by centrifugation, washed several times with absolute ethanol and deionized water. The final product of hollow  $\text{Co}_9\text{S}_8$  nanoparticle was dried in a drying oven at  $80 \text{ }^\circ\text{C}$  for 12 h.

## 2.2 Characterization

The as-prepared samples were characterized on a Shimadzu DX-6000 advanced X-ray powder diffractometer with Cu K $\alpha$  radiation ( $\lambda = 0.15418$  nm) over  $2\theta$  degree from  $10^\circ$  to  $80^\circ$  at a scan rate of  $4^\circ \text{ min}^{-1}$ . The morphology was acquired with a Hitachi (Tokyo, Japan) field-emission scanning electron microscopy (SEM). The nitrogen adsorption-desorption isotherms of the obtained hollow Co<sub>9</sub>S<sub>8</sub> nanospheres were performed using a JW-BK specific surface area instrument (Beijing, China) at 77 K. The specific surface areas were calculated using the Brunauer-Emmett-Teller (BET) method and the pore size distribution curve was acquired based on the Barrett-Johner-Halendar (BJH) model.

## 2.3 Electrochemical measurements

Electrochemical measurements were performed in a three-electrode half-cell setup in 6 M KOH aqueous electrolyte with a CHI 660B workstation (Chenghua, Shanghai, China) operating at room temperature. The working electrode was prepared by mixing the as-prepared hollow Co<sub>9</sub>S<sub>8</sub> nanoparticles powder, BP-2000 carbon and polyvinylidene fluoride (PVDF) in a weight ratio of 7:2:1. The resultant slurry was then coated on the Ni foam (1.0 cm  $\times$  1.0 cm) electrode and allowed to dry at  $80^\circ \text{C}$  for 12 h, resulting in the loading of Co<sub>9</sub>S<sub>8</sub> of about  $3.5 \text{ mg cm}^{-2}$ . A saturated calomel electrode (SCE) and a carbon paper served as reference electrode and counter electrode, respectively. The cyclic voltammetry (CV) curves were examined at a scan rate of  $5 \text{ mV s}^{-1}$  in positive and negative potential windows. Galvanostatic charge/discharge tests were made at current densities of 0.1, 0.5, 1 A  $\text{g}^{-1}$ . The specific capacitance  $C_p$  ( $\text{F g}^{-1}$ ) could be evaluated from the CV curve by Eqn.(1) or from the discharge line by Eqn. (2).

$$C_p = \frac{\int i dV}{m v \Delta V} \quad (1)$$

$$C_p = \frac{I \Delta t}{m \Delta V} \quad (2)$$

where  $I$  (A) is the applied current,  $v$  ( $\text{mV s}^{-1}$ ) is the potential scan rate,  $m$  (g) is the mass of active electrode material,  $\Delta t$  (s) is the discharge time and  $\Delta V$  (V) is the potential window.

Thus, the average energy density  $E$  ( $\text{W h kg}^{-1}$ ) and the average power density  $P$  ( $\text{W kg}^{-1}$ ) were calculated according to the following equations. The parameters in equations are defined as the same as Eqns (1) and (2).

$$E = \frac{1}{2} C_p \Delta V^2 \quad (3)$$

$$P = \frac{E}{\Delta t} \quad (4)$$

## 3. RESULTS AND DISCUSSION

Using sublimed sulfur as sulfur source, hollow Co<sub>9</sub>S<sub>8</sub> nanoparticles were fabricated via solvothermal method, which might result from the slow reaction kinetics of sublimed sulfur with cobalt ion. A typical XRD pattern of the prepared sample is shown in Fig. 1a. It is indicated that all of the diffraction peaks can be clearly indexed as Co<sub>9</sub>S<sub>8</sub> in consistent with JCPDS card No. 19-364 with

face-centered cubic structure, and the broadened diffraction peaks reflect the small sizes of the obtained  $\text{Co}_9\text{S}_8$  sample, which could be evaluated approximately to be ca. 50 nm based on the Debye-Scherrer equation from the most intensive peak (440).[34] SEM image (Fig. 1b) represents further the uniform nanospheres with ca. 50 nm of the obtained  $\text{Co}_9\text{S}_8$  sample, in which some defective nanospheres (marked red circle in SEM image) reveal obviously that the uniform nanospheres are hollow.

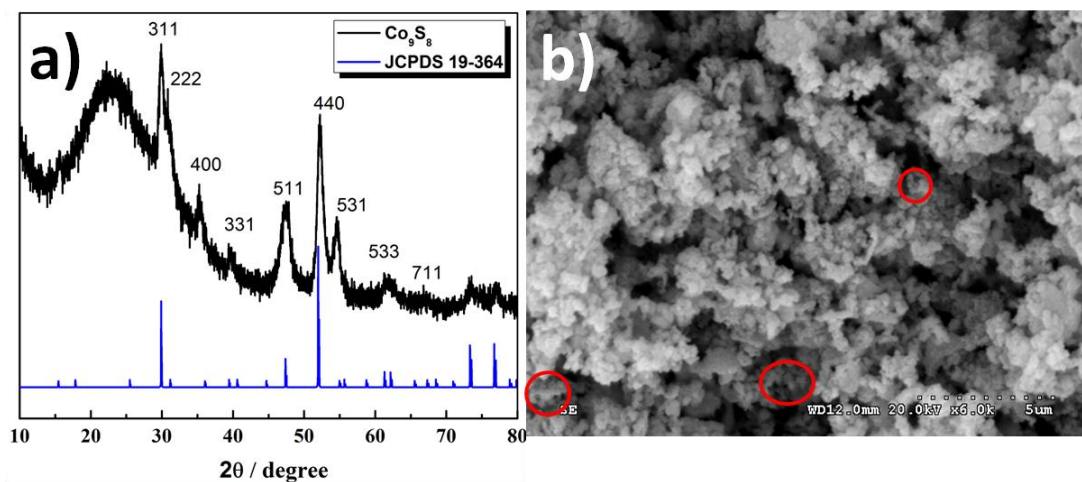


**Figure 1.** (a) Powder X-ray diffraction pattern (a) and SEM image (b) of the prepared hollow  $\text{Co}_9\text{S}_8$  nanospheres.

In order to uncover the property of the hollow  $\text{Co}_9\text{S}_8$  nanospheres, the nitrogen adsorption-desorption isotherm was acquired to estimate the specific area and its pore size distribution (Fig. 2). The similar IV nitrogen adsorption-desorption isotherm allows to result in the specific area of the hollow  $\text{Co}_9\text{S}_8$  nanoparticles to be ca.  $226 \text{ m}^2 \text{ g}^{-1}$  and the pore size distribution (inset in Fig. 2) allows to result in the average pore diameter to be 7.7 nm and the total pore volume to be  $0.434 \text{ cm}^3 \text{ g}^{-1}$ .

The electrochemical performance of the obtained hollow  $\text{Co}_9\text{S}_8$  nanoparticles as supercapacitor was estimated using a three-electrode system in 6 M KOH aqueous solution, with a carbon paper counter electrode and a SCE reference electrode, by Chronopotentiometry, cyclic voltammetry (CV) and electrochemical impedance measurements. Figure 3a shows the typical cyclic voltammograms of the electrode at the first three cycles with a potential window of  $-0.1 - 0.3 \text{ V}$  at a scanning rate of  $5 \text{ mV s}^{-1}$ . As evidenced from the figure, two distinct oxidation peaks (O1, O2) and reduction peaks (R1, R2) exist in all of the curves, indicating the obvious pseudocapacitive features, which is distinguishable from normal electric double-layer capacitance (EDLC) [35-36] with rectangular shape of cyclic voltammogram. The redox mechanism could be explained by the conversion between different cobalt oxidation states proposed by Xu et al.[37], as shown in Eqns.(5) and (6), which is similar to the redox reactions of  $\text{CoS}$  and  $\text{CoS}_2$ [38]. As such, the redox peaks (O1/R1, O2/R2) correspond to the relative redox potential of  $\text{Co}_9\text{S}_8/\text{Co}_9\text{S}_8\text{OH}$  and  $\text{Co}_9\text{S}_8\text{OH}/\text{Co}_9\text{S}_8\text{O}$ , respectively and their good symmetries suggest the reversibility of Eqns (1) and (2). In addition, the CV curves for the first three cycles are almost overlapped, representing the good cycleability of the electrode, and the area under the CV curve allows the evaluation of the specific capacitance of the electrode based on Eqn.(1) to be  $298 \text{ F g}^{-1}$ .

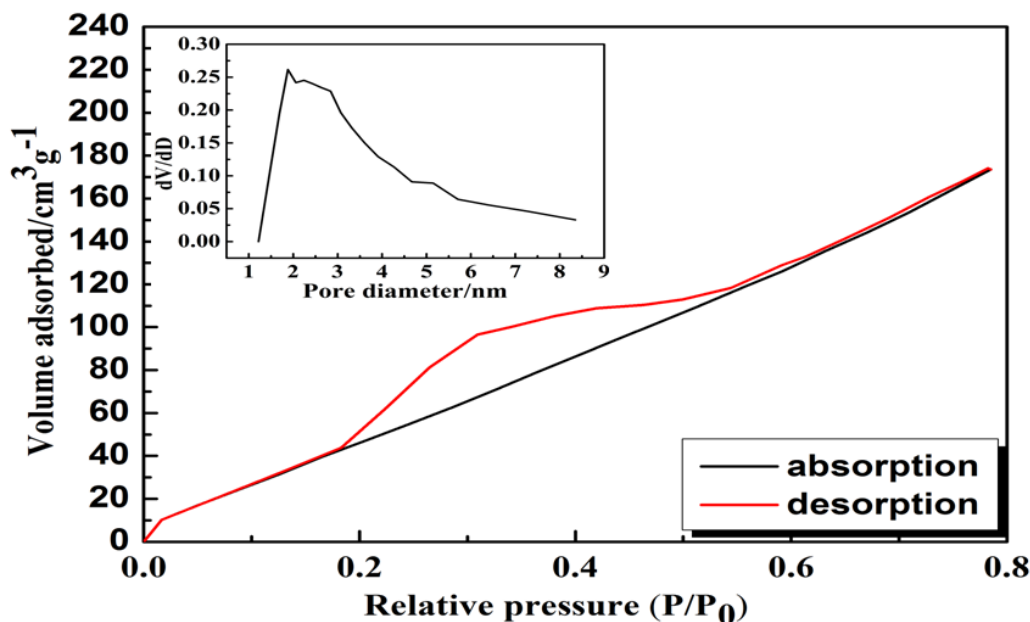


**Figure 2.** The nitrogen gas adsorption-desorption isotherm of  $\text{Co}_9\text{S}_8$  hollow nanosphere. Inset: pore size distribution of  $\text{Co}_9\text{S}_8$  hollow nanosphere.

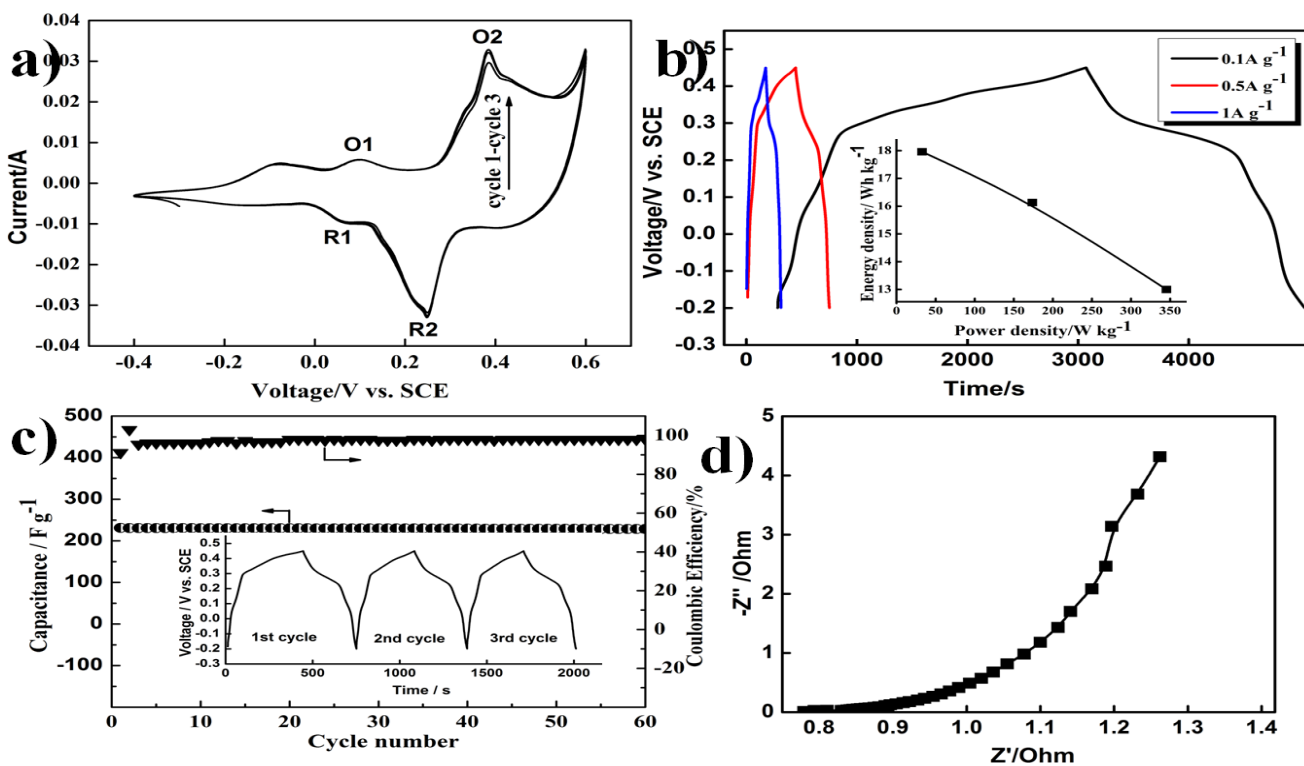
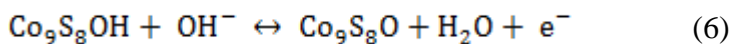
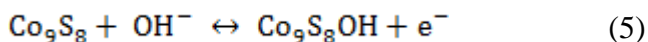


**Figure 3.** (a) Cyclic voltammetric behavior of the prepared  $\text{Co}_9\text{S}_8$  electrode for the first three cycles at  $5 \text{ mV s}^{-1}$  scan rate; (b) Galvanostatic charge/discharge behavior of the prepared  $\text{Co}_9\text{S}_8$  electrode with the potential window of  $0.2 - 0.45 \text{ V}$  at different current density (Inset: Ragone plot of the prepared  $\text{Co}_9\text{S}_8$  electrode); (c) Cyclic performance and Coulombic efficiency of the prepared  $\text{Co}_9\text{S}_8$  electrode at a current density of  $0.5 \text{ A g}^{-1}$  (Inset: the galvanostatic charge/discharge curves for the first three cycles at a current density of  $0.5 \text{ A g}^{-1}$ ); (d) Nyquist plot of the prepared  $\text{Co}_9\text{S}_8$  electrode obtained by applying a sine wave with an AC perturbation of  $5.0 \text{ mV}$  over the frequency range from  $100 \text{ KHz}$  to  $0.01 \text{ Hz}$ .



All these could be further embodied in the galvanostatic charge/discharge behavior using chronopotentiometry. Fig. 3b shows the charge/discharge curves of the obtained  $\text{Co}_9\text{S}_8$  electrode for the initial cycle in the potential range of -0.2 -0.45 V at different current density in 6 M KOH aqueous electrolyte. The two discharge platforms in the discharge curve agree with the two reduction peaks in the above CV curves, demonstrating the typical electrochemical characteristic of pseudocapacitive electrode. [3] Based on Eqn. (2), the specific capacitance could be calculated to be  $306.1 \text{ F g}^{-1}$ ,  $234.7 \text{ F g}^{-1}$  and  $224.0 \text{ F g}^{-1}$  at a current density of  $0.1 \text{ A g}^{-1}$ ,  $0.5 \text{ A g}^{-1}$  and  $1 \text{ A g}^{-1}$ , respectively. It is shown that the initial specific capacitance at  $1 \text{ A g}^{-1}$  is 73.2% of that at  $0.1 \text{ A g}^{-1}$  and 95.4 % at  $0.5 \text{ A g}^{-1}$ , revealing the good rate property of the prepared hollow  $\text{Co}_9\text{S}_8$  nanosphere electrode for the supercapacitor. This might be mainly attributed to the shortened path for the electronic transport and the ionic diffusion between the electrolyte and the electrode surface due to the hollow  $\text{Co}_9\text{S}_8$  nanospheres. [39-40] As shown in the inset of Fig. 3b for the Ragone plot [1-2, 5, 17] to delineate the relationship of the energy density and the power density calculated in terms of Eqns (3) and (4), the prepared hollow  $\text{Co}_9\text{S}_8$  nanosphere electrode may deliver a high energy density of  $17.96 \text{ Wh kg}^{-1}$  at a power density of  $32.82 \text{ W kg}^{-1}$  and still maintains  $13 \text{ Wh kg}^{-1}$  at a higher power density of  $345.28 \text{ W kg}^{-1}$ , manifesting the unique characteristic of pseudocapacitive material to improve the energy density at a high power density. The electrochemical stability of the prepared  $\text{Co}_9\text{S}_8$  electrode was also conducted for 60 continuous cycles at a current density of  $0.5 \text{ A g}^{-1}$ , as shown in Fig. 3c. It can be seen that the specific capacitance could be kept at  $\sim 234.5 \text{ F g}^{-1}$  up to the 60th cycling, which is consistent with the above CV results and could also be further verified by the charge/discharge behavior, as shown in the inset of Fig. 3c for the charge/discharge curves of the first three cycles at a current density of  $0.5 \text{ A g}^{-1}$  to deliver a specific capacitance of 234.7, 234.5,  $234.3 \text{ F g}^{-1}$ , respectively. Furthermore, Coulombic efficiency was also recorded in Fig. 3c and maintains a stable high value of 98% except for the somewhat dramatic change at the first two cycles due to the activation process of the electrode material. Electrochemical impedance spectroscopy (EIS) analysis with AC perturbation of 5 mV in the frequency range of 100 kHz to 0.01 Hz at an open circuit potential (OCV) has been used to dissect the above mentioned electrochemical performance of the prepared  $\text{Co}_9\text{S}_8$  electrode.[41] As shown in Fig. 3d, the flat-like semicircle in the high frequency region in the Nyquist plot reflects a small diameter of the circle, indicating the small interfacial charge transfer resistance and thus the improved conductivity of the prepared electrode material. This might be due to the short path of the hollow  $\text{Co}_9\text{S}_8$  nanosphere for the electronic transportation and the ionic diffusion.

#### 4. CONCLUSIONS

The hollow  $\text{Co}_9\text{S}_8$  nanospheres with ca. 50 nm in diameter were fabricated successfully by a facile solvothermal method to yield a specific area of  $226 \text{ m}^2 \text{ g}^{-1}$  and an average pore size of 7.7 nm.

The electrochemical performance of the prepared hollow Co<sub>9</sub>S<sub>8</sub> nanospheres as a pseudocapacitor electrode was estimated using a three electrodes system. The prepared hollow Co<sub>9</sub>S<sub>8</sub> nanospheres electrode delivers a specific capacitance of 306.1 F g<sup>-1</sup>, 234.7 F g<sup>-1</sup> and 224.0 F g<sup>-1</sup> at a current density of 0.1 A g<sup>-1</sup>, 0.5 A g<sup>-1</sup> and 1 A g<sup>-1</sup>, respectively, indicating a good rate capability. More importantly, the energy density is enhanced greatly at a certain power density, exhibiting a typical pseudocapacitive characteristic. All these might be attributed to the short path of the electronic transportation and the ionic diffusion due to the unique hollow Co<sub>9</sub>S<sub>8</sub> nanospheres, as demonstrated by EIS analysis. Therefore, Co<sub>9</sub>S<sub>8</sub> as a pseudocapacitor electrode exhibits a promising application in energy storage

#### ACKNOWLEDGEMENTS

This work was supported by Hubei Provincial Natural Science Foundation of China (No. 2015CFC842), Education Science Foundation of Hubei Province (No. T200908), Project of Chinese Ministry of Education (No. 208088).

#### References

1. R. Kötz and M. Carlen, *Electrochim. Acta*, 45(2000)2483.
2. P. Simon and Y. Gogotsi, *Nat. Mater.*, 7(2008)845.
3. G. Wang, L. Zhang and J. Zhang, *Chem. Soc. Rev.*, 41(2012)797.
4. P. Simon and Y. Gogotsi, *Philos. Transact. A Math. Phys. Eng. Sci.*, 368(2010)3457.
5. P. Simon and Y. Gogotsi, *Acc. Chem. Res.*, 46(2013)1094.
6. Y. Wang, Z. Q. Shi, Y. Huang, Y. F. Ma, C. Y. Wang, M. M. Chen and Y. S. Chen, *J. Phys. Chem. C*, 113(2009)13103.
7. Y.-g. Wang and Y.-y. Xia, *Electrochem. Commun.*, 7(2005)1138.
8. Q. Zhang, E. Uchaker, S. L. Candelaria and G. Cao, *Chem. Soc. Rev.*, 42(2013)3127.
9. B. Gao, X. Li, Y. Ma, Y. Cao, Z. Hu, X. Zhang, J. Fu, K. Huo and P. K. Chu, *Thin Solid Films*, 584(2015)61.
10. S. Ullah, I. A. Khan, M. Choucair, A. Badshah, I. Khan and M. A. Nadeem, *Electrochim. Acta*, 171(2015)142.
11. C. Wang, F. Li, Y. Wang, H. Qu, X. Yi, Y. Lu, Y. Qiu, Z. Zou, B. Yu and Y. Luo, *J. Alloys Compd.*, 634(2015)12.
12. C. Wu, J. Cai, Q. Zhang, X. Zhou, Y. Zhu, L. Li, P. Shen and K. Zhang, *Electrochim. Acta*, 169(2015)202.
13. C. Yuan, L. Hou, Y. Feng, S. Xiong and X. Zhang, *Electrochim. Acta*, 88(2013)507.
14. G. G. Amatucci, F. Badway, A. Du Pasquier and T. Zheng, *J. Electrochem. Soc.*, 148(2001)A930.
15. H.-L. Girard, H. Wang, A. d'Entremont and L. Pilon, *J. Phys. Chem. C*, 119(2015)11349.
16. S. Kim, J. Lee, J. S. Kang, K. Jo, S. Kim, Y. E. Sung and J. Yoon, *Chemosphere*, 125(2015)50.
17. K. Naoi, W. Naoi, S. Aoyagi, J.-i. Miyamoto and T. Kamino, *Acc. Chem. Res.*, 46(2013)1075.
18. B. Vidyadharan, I. I. Misnon, J. Ismail, M. M. Yusoff and R. Jose, *J. Alloys Compd.*, 633(2015)22.
19. H. BináWu, *Chem. Commun.*, 48(2012)6912.
20. K. Dai, D. Li, L. Lu, Q. Liu, J. Lv and G. Zhu, *RSC Adv.*, 4(2014)29216.
21. S. Peng, L. Li, H. Tan, R. Cai, W. Shi, C. Li, S. G. Mhaisalkar, M. Srinivasan, S. Ramakrishna and Q. Yan, *Adv. Funct. Mater.*, 24(2014)2155.
22. B. Wang, J. Park, D. Su, C. Wang, H. Ahn and G. Wang, *J. Mater. Chem.*, 22(2012)15750.
23. J.-C. Xing, Y.-L. Zhu, M.-Y. Li and Q.-J. Jiao, *Electrochim. Acta*, 149(2014)285.
24. P. F. Yin, L. L. Sun, Y. L. Gao and S. Y. Wang, *Bull. Mater. Sci.*, 31(2008)593.

25. X. F. Qian, X. M. Zhang, C. Wang, Y. Xie and Y. T. Qian, *Inorg. Chem.*, 38(1999)2621.
26. Y. X. Zhou, H. B. Yao, Y. Wang, H. L. Liu, M. R. Gao, P. K. Shen and S. H. Yu, *Chemistry*, 16(2010)12000.
27. Y. Yin, R. M. Rioux, C. K. Erdonmez, S. Hughes, G. A. Somorjai and A. P. Alivisatos, *Science*, 304(2004)711.
28. I. Bezverkhyy, P. Afanasiev and M. Danot, *The Journal of Physical Chemistry B*, 108(2004)7709.
29. R. A. Sidik and A. B. Anderson, *J. Phys. Chem. B*, 110(2006)936.
30. J. Wang, S. H. Ng, G. X. Wang, J. Chen, L. Zhao, Y. Chen and H. K. Liu, *J. Power Sources*, 159(2006)287.
31. R. Ramachandran, M. Saranya, C. Santhosh, V. Velmurugan, B. P. Raghupathy, S. K. Jeong and A. N. Grace, *RSC Adv.*, 4(2014)21151.
32. J. Pu, Z. Wang, K. Wu, N. Yu and E. Sheng, *Phys. Chem. Chem. Phys.*, 16(2014)785.
33. J. Wen, S. Li, B. Li, Z. Song, H. Wang, R. Xiong and G. Fang, *J. Power Sources*, 284(2015)279.
34. Y. R. Wang, J. Wang, H. T. Liao, X. F. Qian, M. Wang, G. S. Song and S. Q. Cheng, *RSC Adv.*, 4(2014)3753.
35. F. Zhang, T. Zhang, X. Yang, L. Zhang, K. Leng, Y. Huang and Y. Chen, *Energ. Environ. Sci.*, 6(2013)1623.
36. K. Xie, X. Qin, X. Wang, Y. Wang, H. Tao, Q. Wu, L. Yang and Z. Hu, *Adv. Mater.*, 24(2012)347.
37. J. Yu, H. Wan, J. Jiang, Y. Ruan, L. Miao, L. Zhang, D. Xia and K. Xu, *J. Electrochem. Soc.*, 161(2014)A996.
38. B. Wang, J. Park, D. Su, C. Wang, H. Ahn and G. Wang, *J. Mater. Chem.*, 22(2012)15750.
39. A. Walcarius, *Chem. Soc. Rev.*, 42(2013)4098.
40. K. Torchała, K. Kierzek, G. Gryglewicz and J. Machnikowski, *Electrochim. Acta*, 167(2015)348.
41. X. F. Qian, Y. R. Wang, W. Zhou, L. P. Zhang, G. S. Song and S. Q. Cheng, *Int. J. Electrochem.Sci.*, 10(2015)3510.